Effect of Al_2O_3/SiO_2 Ratio on Structure and Properties of Mould Flux for High-Al Steel Continuous Casting

Qi Wang[1,2], Jianqiang Zhang[1], Oleg Ostrovski[1], Chen Zhang[3], Dexiang Cai[3]*

1. The University of New South Wales, Sydney, 2052 Australia.
2. Midea Group Laundry Appliance Division, Wuxi, Jiangsu, 214028 China
3. Baosteel Group Corporation Research Institute, Baoshan, Shanghai, 201900 China
* Corresponding author E-mail: j.q.zhang@unsw.edu.au

Keywords: Al_2O_3/SiO_2 ratio, mould flux, high-Al steel, continuous casting.

ABSTRACT

The conventional $CaO-SiO_2$-based mould fluxes are not suitable for high-Al steel casting because of the strong reaction between silica in the flux and aluminium in the steel strand. In the process of casting of high-Al steel, flux composition changes; with the decrease of the silica concentration and increase of alumina. Knowledge and understanding of the effect of the Al_2O_3/SiO_2 ratio on flux structure and properties are useful for flux design for the high Al-steel continuous casting.

This paper investigated the effect of the Al_2O_3/SiO_2 ratio on structure, viscosity, phase composition of fluxes quenched at different temperatures and heat transfer of $CaO-Al_2O_3-SiO_2-B_2O_3-Na_2O-Li_2O-MgO-F$ fluxes. It was found that flux melting temperature increased with the increase in Al_2O_3/SiO_2 ratio. Viscosity of the flux melts increased significantly with the increase of the Al_2O_3/SiO_2 ratio from 0.7 to 1.2, reaching the maximum value, and then decreased with further increase of the Al_2O_3/SiO_2 ratio. Raman spectroscopy analysis revealed that the change of the Al_2O_3/SiO_2 ratio led to the change of aluminate and silicate structural units. The turning point for viscosity was attributed to the change in the degree of flux polymerisation. XRD analysis showed that increasing Al_2O_3/SiO_2 ratio increased crystallisation tendency of the fluxes. Heat transfer measurement by infrared emitter technique (IET) revealed that increasing Al_2O_3/SiO_2 ratio led to the decrease in heat flux which is correlated well with the increased crystallinity of the flux. The results suggested that the flux with Al_2O_3/SiO_2 ratio 4.3 is the best candidate among the studied $CaO-Al_2O_3$-based mould fluxes for casting of high-Al steel.

INTRODUCTION

Conventional $CaO-SiO_2$-based mould fluxes contain high concentrations of SiO_2 (up to 56 mass pct [Brandaleze et al. 2012]) which is essential to ensure the required flux properties for steel casting. However, for casting of high aluminium steel such as advanced high strength steel (0.5-2.0 mass pct Al), [Al] in the steel can react with (SiO_2) in the flux, increasing the Al_2O_3 content and decreasing the SiO_2 content in the mould flux, i.e. increasing the ratio of Al_2O_3/SiO_2. As a result, it leads to an inevitable variation of flux properties, and consequently, affecting the casting of high-Al steel [Kim et al. 2013, Cho et al. 2013, Kang et al. 2013, Chung and Cramb 2000, Zhou et al. 2017, Zhou et al. 2015].

This work investigated the effect of Al_2O_3/SiO_2 ratio on the physicochemical properties, structure, and heat transfer of mould fluxes for continuous casting of high-Al steel. The ratio of Al_2O_3/SiO_2 changed from a relatively low value to a high one to reflect the flux composition change during high-Al steel casting process. The information of the effect of this ratio on flux structure and properties is useful for the flux design for high Al-steel continuous casting.

MATERIALS AND EXPERIMENTAL PROCEDURE

Materials

Flux samples were prepared by using reagent grade $CaCO_3$, Na_2CO_3, Li_2CO_3, SiO_2, Al_2O_3, B_2O_3 and CaF_2 which were fully mixed, and then melted in a high-purity graphite crucible at 1400 °C for 20 minutes. After that, the melted flux was quenched into water, then dried at 120 °C for 2h, and ground into fine powders using a ring mill. The contents of B_2O_3 and Li_2O were analyzed using inductively coupled plasma (ICP, Thermo Scientific IRIS Intrepid II, MA), while the other flux components were determined by X-ray fluoroscopy (XRF, PANalytical AXIOS-Advanced WDXRF spectrometer, Netherland). The measured flux compositions are shown in **Table 1.** The Al_2O_3/SiO_2 ratio of fluxes varied from 0.7 to 10.8 while concentrations of all other components were set as constants. All 5 flux samples are based on the $CaO-Al_2O_3-SiO_2-B_2O_3$ quaternary system with the addition of Na_2O, Li_2O, MgO, and F. It should be mentioned that variation of the Al_2O_3/SiO_2 mass ratio changed the CaO/Al_2O_3 mass ratio within the range 2.2-1.1.

Table 1. Measured chemical composition of mould fluxes, mass pct. and Al_2O_3/SiO_2 ratio

Flux	CaO	Al_2O_3	SiO_2	Na_2O	B_2O_3	Li_2O	MgO	F	Al_2O_3/SiO_2
1	32.7	15.1	21.5	6.0	12.4	3.9	2.1	6.3	0.7

2	32.6	19.8	16.5	6.1	12.7	3.8	2.0	6.5	1.2
3	33.2	24.6	11.8	6.1	11.7	3.7	2.1	6.8	2.1
4	31.6	30.0	7.0	6.2	12.7	4.1	2.0	6.3	4.3
5	33.6	32.0	2.9	6.4	12.4	4.0	2.1	6.5	10.8

Experimental Procedure

Melting properties of mould fluxes were investigated using a hot stage microscopy. As-quenched flux powders were pressed to pellets (Φ 3×3 mm). The pellets were continuously heated in a horizontal tube furnace at a rate of 15 °C/min; their appearance change was monitored by a video camera. To characterize the melting properties of mould fluxes, the softening, hemispherical, and fluidity temperatures were defined as the temperatures at which the height of the flux pellet dropped to 75, 50 and 25 pct of its original height, respectively. The details of melting property measurement were described elsewhere [Yang et al. 2018, Yang et al. 2017].

Viscosity of mould fluxes was investigated using a rotation viscometer (model ZC-1600, China). Approximately 140 g pre-melted flux was heated up to 1400 °C in a graphite crucible in nitrogen atmosphere. After holding the molten flux at 1400 °C for 1200 seconds, a Mo bob was slowly submerged into the homogenized melt and rotated at a rate of 12 rpm for the measurement of viscosity. After measurement of the flux viscosity at 1400 °C, the viscosity was measured in the process of flux continuous cooling with a rate of 5 °C/min until the Mo bob stopped rotation.

The structure of as-quenched mould fluxes from 1400 °C was studied using Raman spectroscopy (Renishaw inVia Raman Microscope, UK). The pulverized mould flux was illuminated by Ar-ion laser beam. The excitation wavelength of Ar-ion laser was 514 nm with a beam spot size of 1.5 μm. The measurement was conducted in the Raman shift range from 400 to 1700 cm^{-1}. The obtained Raman spectra were deconvoluted using WiRE 4.4 software.

The heat transfer rate across the mould fluxes was measured using infrared emitter technique (IET, Central South University, China). The details of IET system were described elsewhere [Wang and Cramb 2005]. The flux disk was prepared using 13 g as-quenched flux powders which were melted at 1400 °C and held for 1200 seconds before pouring into a copper cylinder (Φ 40 mm) and pressing to a disk. The pressed mould flux disk was immediately placed in a muffle furnace in which the temperature gradually decreased from 800 °C to 25 °C with a slow cooling rate of 1 °C/min to minimize the internal stress within the disk. The fabricated flux disk was ground to the thickness of 4 ± 0.01 mm using a diamond grinding wheel, and then carefully polished using sandpapers from 300 to 1200 grits. In the heat flux measurement, the mould flux disk was placed on the copper base of the IET system. The incident thermal radiation was increased up to 1.6 MW/m^2, which is close to the radiation released from the steel strand in the continuous casting. The temperatures recorded by the embedded thermocouples were used for the heat flux calculation according to the Fourier's law [Park et al. 2016]:

$$q = \frac{-1}{n}\sum_i k\left(\frac{dT}{dx}\right)_i \quad (1)$$

where q is the heat flux, n presents the total number of thermocouples, k is the thermal conductivity of copper. The heat fluxes measured at an incident radiation of 1.6 MW/m^2 were compared to reflect the heat transfer ability of fluxes during continuous casting.

The crystalline phases in the mould fluxes heated to different temperatures and quenched were determined using X-ray diffraction (XRD) with Cu-Kα radiation in the scanning range of 2θ from 10 to 80 deg with a scanning speed of 0.021 deg/s. Eight-gram samples for the XRD analyses were prepared separately by holding the fluxes at 950 °C (low temperature zone), 1050 °C (medium temperature zone), and 1150 °C (high temperature zone) for 30 minutes. Then the heat-treated samples were quenched into water and subjected to the XRD analysis. The selection of these three temperatures was based on the TTT measurement to reflect the phase changes at low, medium and high temperatures. The XRD spectra were analysed using HighScore Plus 4.2.

RESULTS

Melting properties

Figure 1 illustrates the influence of Al_2O_3/SiO_2 ratio on softening temperature (T_s), hemispherical temperature (T_h) and fluidity temperature (T_f) of the CaO-Al_2O_3-based mould fluxes.

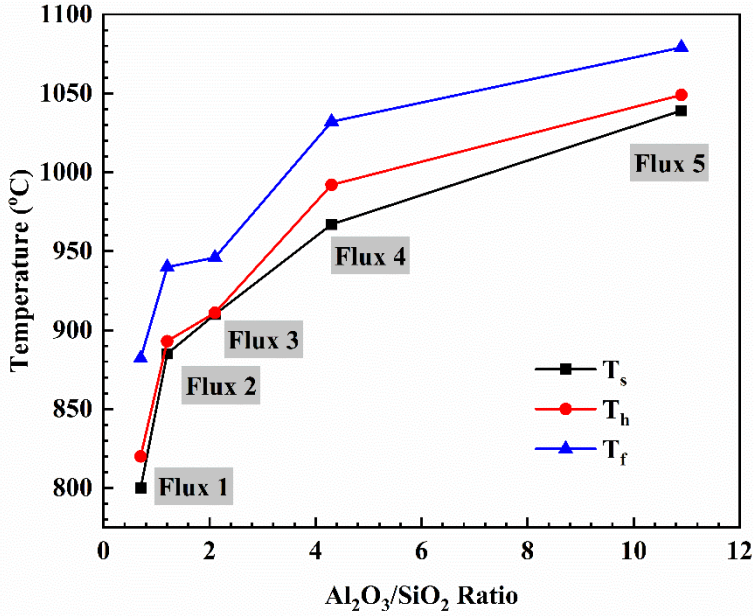

Fig. 1 Softening temperature (T_s), hemispherical temperature (T_h) and fluidity temperature (T_f) as functions of the Al_2O_3/SiO_2 ratio.

With the increase in the mass ratio of Al_2O_3/SiO_2 from 0.7 to 10.8, all three characteristic temperatures T_S, T_h and T_f continuously increased (**Figure 1**). The value of T_f is much higher than those of T_s and T_h in all cases.

Viscosity

Figure 2 shows the measured viscosity as a function of temperature. It was observed that for all mould fluxes, viscosity increased with the decrease in temperature. The enlarged scale of viscosity in the high-temperature zone from 1300 to 1400 °C is shown in **Figure 3**. It was observed that when increasing the mass ratio of Al_2O_3/SiO_2 from 0.7 to 1.2, the viscosity increased significantly. With further increasing this ratio, the viscosity decreased. As a result, Flux 8-2 had the highest viscosity in all the fluxes. The viscosities at 1400 °C (η_{1400}) of all examined mould fluxes are presented in **Table 2,** further confirming that the viscosity reaches the highest point when Al_2O_3/SiO_2 = 1.2, and reduces gradually with further increase in Al_2O_3/SiO_2 ratio.

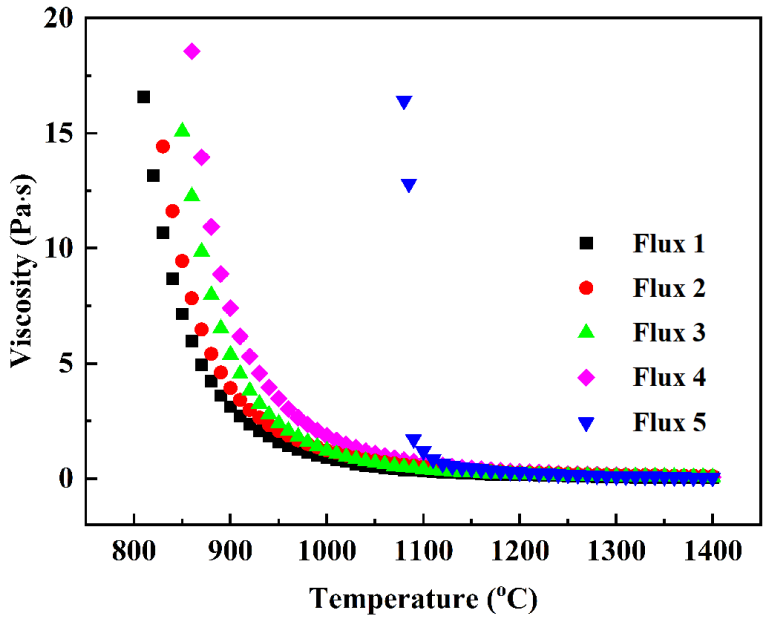

Fig. 2 Viscosity of mould flux with different Al_2O_3/SiO_2 ratios at different temperatures

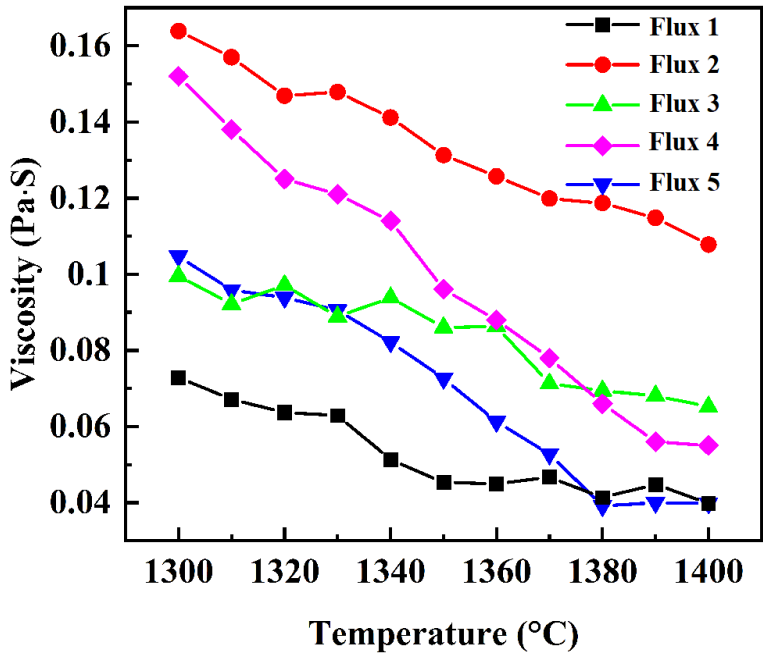

Fig. 3 Highlight the viscosity at temperatures 1300 – 1400 °C

Liquid flux can be assumed to be a Newtonian fluid and its viscosity can be fitted by the Arrhenius equation.

$$\ln \eta = \ln A + \frac{Ea}{RT} \tag{2}$$

Where η represents viscosity; A is viscosity constant; T is the temperature, and Ea activation energy.

Figure 4 shows the Arrhenius plot of $\ln\eta$ as a function of $1/T$. It appears that only Flux 5 shows a clear break temperature at 1105 °C, while all other fluxes do not have apparent break temperatures. The activation energies determined in the temperature range of 1100-1330°C are 137 kJ·mol^{-1} for Flux 1, 98 kJ·mol^{-1} for Flux 2, 117 kJ·mol^{-1} for Flux 3, 156 kJ·mol^{-1} for Flux 4, and 188 kJ·mol^{-1} for Flux 5 in temperature range of 1100-1330°C. All these results are shown in **Table 2.**

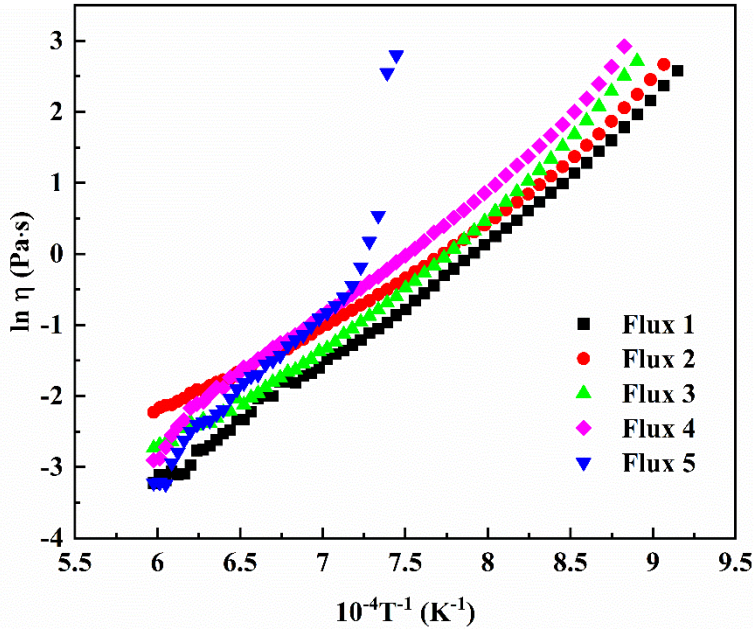

Fig. 4 Plots of $\ln\eta \; vs \; \frac{1}{T}$ for fluxes with Al_2O_3/SiO_2 ratio increased from 0.7 to 10.8.

Table 1 Calculated apparent activation energy (*E*a), break temperature (T_{br}), and viscosity at 1400 °C (η_{1400}) for the fluxes with different Al_2O_3/SiO_2 ratios

Flux	*Ea* (kJ·mol^{-1})	R^2	T_{br}, °C	η_{1400}, Pa·s
1	137	0.991	-	0.040
2	98	0.996	-	0.108
3	117	0.989	-	0.065
4	156	0.978	-	0.055
5	188	0.985	1105	0.039

Raman analysis

The structure of mould flux with varying Al_2O_3/SiO_2 mass ratios was studied using the Raman spectroscopy. **Figure 5** illustrates the Raman spectra of as-quenching mould fluxes and **Table 3** lists the assignments of deconvoluted Raman bands. In the low frequency region (between 400 and 800 cm^{-1}) the deconvoluted bands were assigned to aluminate group in which peaks around 500 cm^{-1} were assigned to Al-F stretching vibration in AlF_6; peaks centered around 550 cm^{-1} correspond to Al-O-Al linkage which is the major bond in the 3-D aluminate network; peaks located around 590 cm^{-1} are related to Al-O$^-$ stretching vibration in AlO_6 units; peaks located around 770 cm^{-1} are related to Al-O$^-$ stretching vibration in Al-NBO units with 1 or 2 NBOs (non-bridging oxygen); peaks centered around 865 cm^{-1} correspond to Al-O-Si linkage. Among these characteristic peaks, structural units with Al-O-Si and Al-O-Al linkages had the most prominent peaks; with the increase of Al_2O_3/SiO_2 mass ratio, peaks assigned to AlF_6 and Al-O-Al linkages became more and more prominent, while peaks assigned to Al-O-Si linkage became weaker.

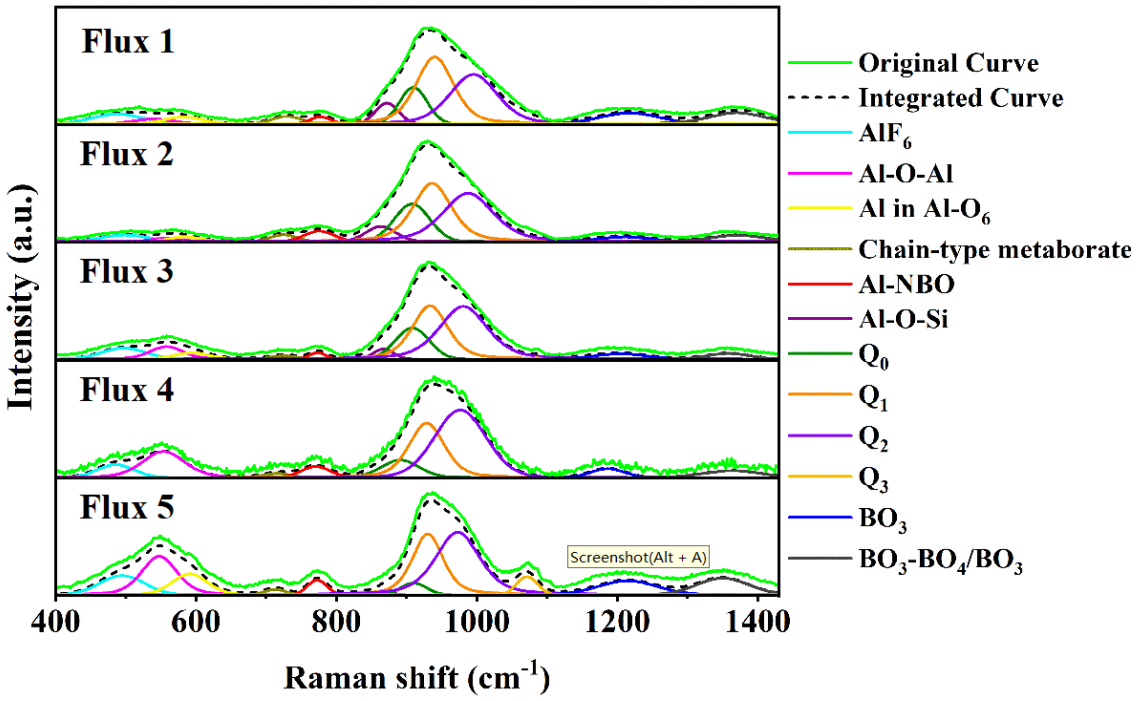

Fig. 5 Deconvoluted Raman spectra for mould flux with various Al_2O_3/SiO_2 ratios

Table 2 Assignments of deconvoluted Raman bands

Flux 1	Flux 2	Flux 3	Flux 4	Flux 5	Structural unit	Ref.
488.1	498.5	497.0	485.2	494.3	AlF_6	Park 2002, Ma 2018
539.3	558.0	557.8	553.5	547.5	Al-O-Al	Park 2002
582.2	584.1	594.2	-	590.9	AlO_6	Park 2002, McMillan 1983
729.2	724.4	724.7	715.6	712.9	Chain-type metaborate	Kim 2014, Kamitsos 1987
777.0	775.4	772.9	770.2	772.4	Al-NBO	Gao 2017, Kim 2014
872.0	863.1	866.8	851.0	870.4	Al-O-Si	Gao 2016A, Gao 2016B
909.5	907.0	908.0	890.9	910.0	Q^0	Kim 2012, Zheng 2014
940.0	936.2	933.3	928.5	930.0	Q^1	
995.1	987.4	980.7	976.3	972.6	Q^2	
-	-	-	--	1071.5	Q^3	
1217.8	1210.9	1205.0	1186.3	1214.8	BO_3	Kim 2014, Kamitsos 1987
1370.7	1371.8	1358.1	1364.2	1350.3	BO_3-BO_4/BO_3	

In the medium frequency range (900 to 1100 cm^{-1}), the deconvoluted Raman peaks were assigned to silicate structures, including Si-O stretching vibration in SiO_4^{4-} (Q^0), $Si_2O_7^{6-}$ (Q^1), SiO_3^{2-} (Q^2) and $Si_2O_5^{2-}$ (Q^3). In all fluxes, Q^1 and Q^2 were the dominant units, Q^0 and Q^3 were less noticeable in the Raman spectra. No Q^4 unit was detected for all fluxes. Based on the spectra profile between 900 and 1100 cm^{-1} (**Figure 5**), with the increase of Al_2O_3/SiO_2 ratio, the area fraction of Q^0 decreased while the fraction of Q^2 increased, which means the simple silicate structure became less significant with the increase of Al_2O_3/SiO_2 mass ratio; the fraction of Q^1 did not change.

In the high frequency range, the Raman bands were assigned to different borate structures, where the peaks around 1210 cm^{-1} correspond to the B-O stretching vibration in BO_3 units which was a necessary component to form 3-D borate groups, while the peak around 1360 cm^{-1} was assigned to B-O stretching vibration in BO_3^- units attached to other 3-D borate groups. There is also a borate band located around 720 cm^{-1}, corresponding to chain-type metaborate groups. With the increase of Al_2O_3/SiO_2 ratio from 0.7 to 1.2, the fractions of these two borate units became depressed; with further increase the ratio to 10.8, the fractions of these units gradually increased.

The percentage of some main peaks from deconvoluted Raman spectra is shown in **Figure 6**. Increasing Al_2O_3/SiO_2 ratio increased the fraction of Al-O-Al, AlF_6 and Q^2, but decreased that of Q^0, Al-O-Si. The fraction of Q^1 remained no change.

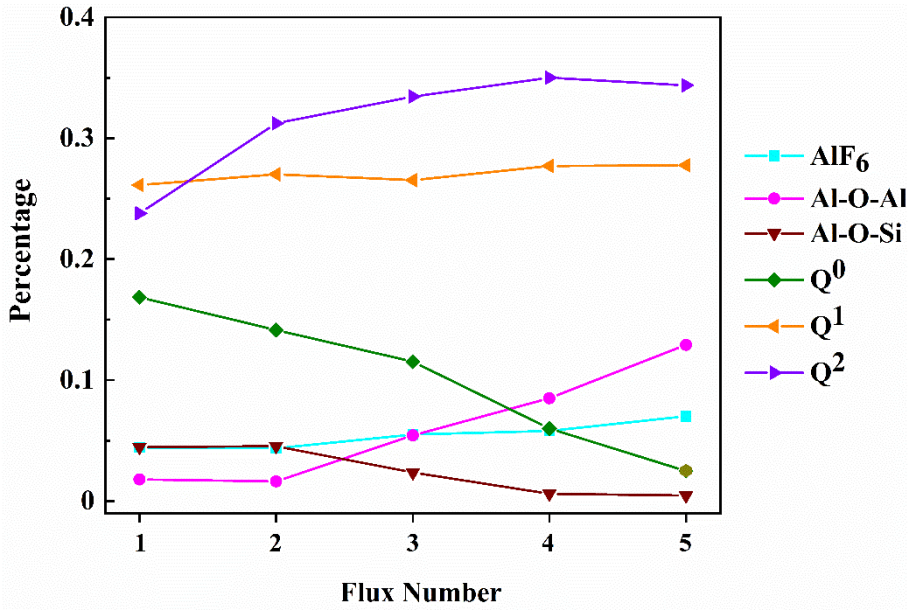

Fig. 6 Percentage of main peaks based on the deconvoluted Raman spectra

Flux phase analysis by XRD

Figure 7 and **Figure 8** show the XRD patterns of mould fluxes 1 to 5 heat treated at 900 °C and 1000 °C; the XRD patterns of Flux 4 heat-treated at 950 °C and 1050 °C were also shown in these two figures, respectively. **Table 4** lists the crystal phases identified by XRD at different temperatures. For Fluxes 2 and 3 (Al_2O_3/SiO_2 ratio of 1.2 and 2.1, respectively), $Ca_2Al_2SiO_7$ was the only phase at both 900 °C and 1000 °C. However, for other fluxes, different phases formed. At 900 °C, $Ca_4Si_2O_7F_2$ (cuspidine) was detected to be the main phase in Flux 1 with Al_2O_3/SiO_2 ratio of 0.7, while the crystalline phases of Flux 5 with Al_2O_3/SiO_2 ratio of 10.8 were $Ca_5B_3O_9F$, $CaSiO_3$ and $LiAlO_2$ ($LiAlO_2$ was the main phase). For Flux 4, $Ca_2Al_2SiO_7$, $MgAl_6O_{10}$, $LiAlO_2$ were detected at 950 °C. At 1000 °C, the crystal phases detected in Flux 4 were the same as those at 900 °C, while there was only trace amount of $Ca_4Si_2O_7F_2$ (cuspidine) detected in amorphous matrix for Flux 1 after heat treatment at 1000 °C. For Flux 4 at 1050°C, $MgAl_6O_{10}$, $LiAlO_2$, and $Ca_2Al_2SiO_7$ were identified.

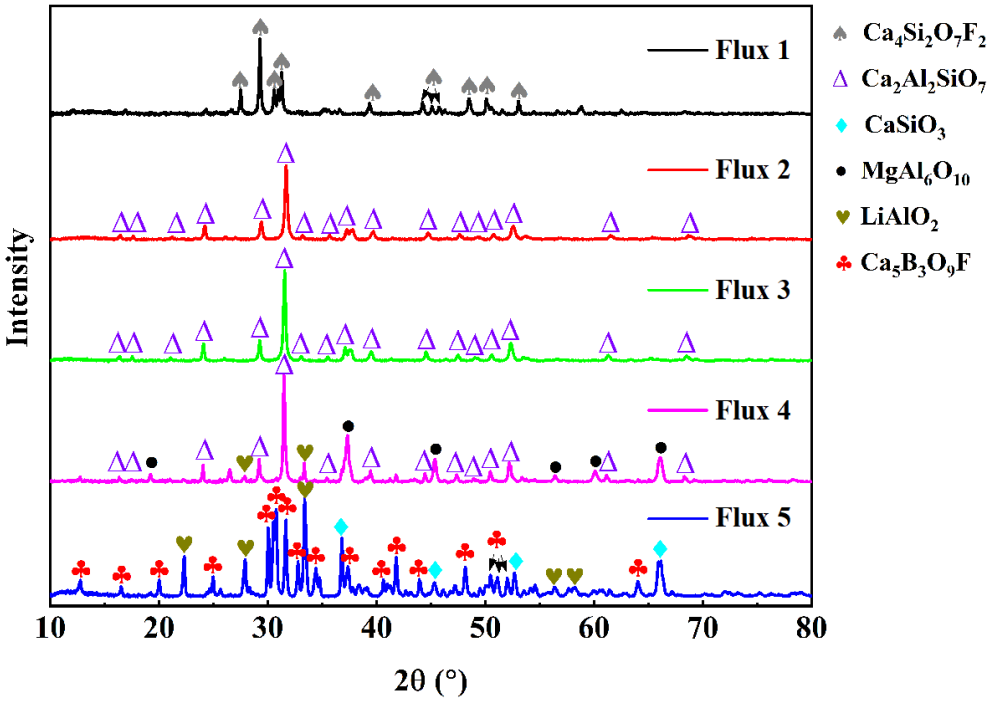

Fig. 7 XRD patterns of Fluxes 1, 2, 3 and 5 heated at 900 °C and Flux 4 at 950 °C

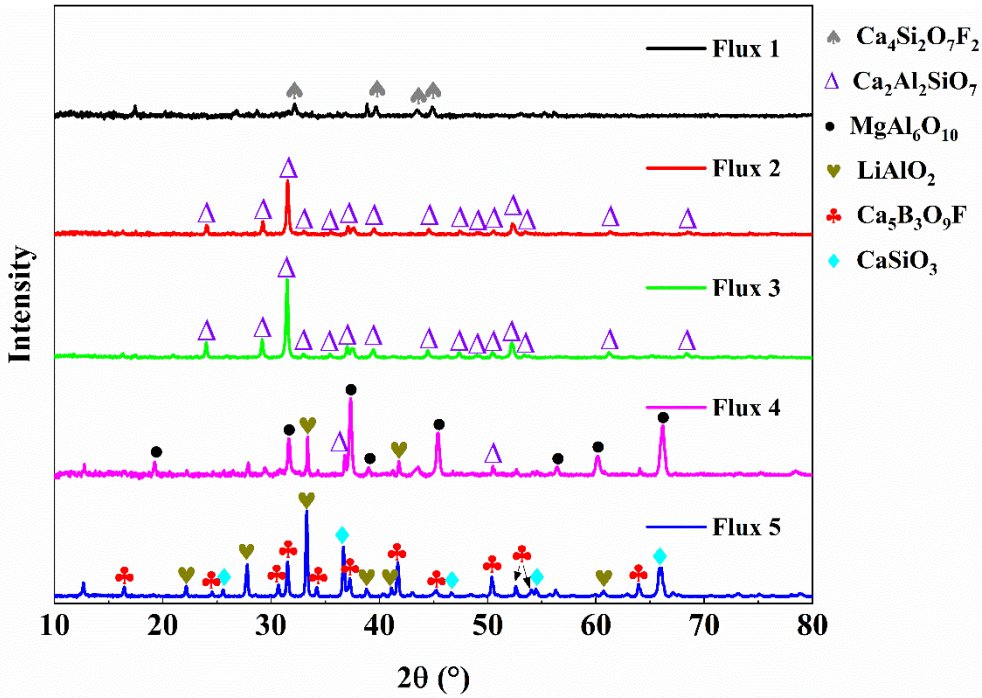

Fig. 8 XRD patterns of Fluxes 1, 2, 3 and 5 heated at 1000 °C and Flux 4 at 1050 °C

Table 3 Summary of the XRD results at different temperatures

T/°C	900	1000
Flux 1	$Ca_4Si_2O_7F_2$	Amorphous + trace amount of $Ca_4Si_2O_7F_2$
Flux 2	$Ca_2Al_2SiO_7$	$Ca_2Al_2SiO_7$
Flux 3	$Ca_2Al_2SiO_7$	$Ca_2Al_2SiO_7$
Flux 4	(950°C) $Ca_2Al_2SiO_7$, $MgAl_6O_{10}$, $LiAlO_2$	(1050°C) $MgAl_6O_{10}$, $LiAlO_2$, $Ca_2Al_2SiO_7$

Flux 5	$LiAlO_2$, $Ca_5B_3O_9F$, $CaSiO_3$	$LiAlO_2$, $CaSiO_3$, $Ca_5B_3O_9F$

Heat transfer of mould flux

Figure 9 shows results of IEF experiments for five mould fluxes. The heat flux tended to be stable after 2100 seconds. The average heat flux values of the five fluxes at the final stage were 760.6, 720.0, 700.1, 686.0, 440.3 kW/m^2, respectively. It means that with the increase of Al_2O_3/SiO_2 ratio from 0.7 to 10.8 the heat flux decreases. Among these values, the heat flux for Flux 5 had a much lower value than those for other fluxes.

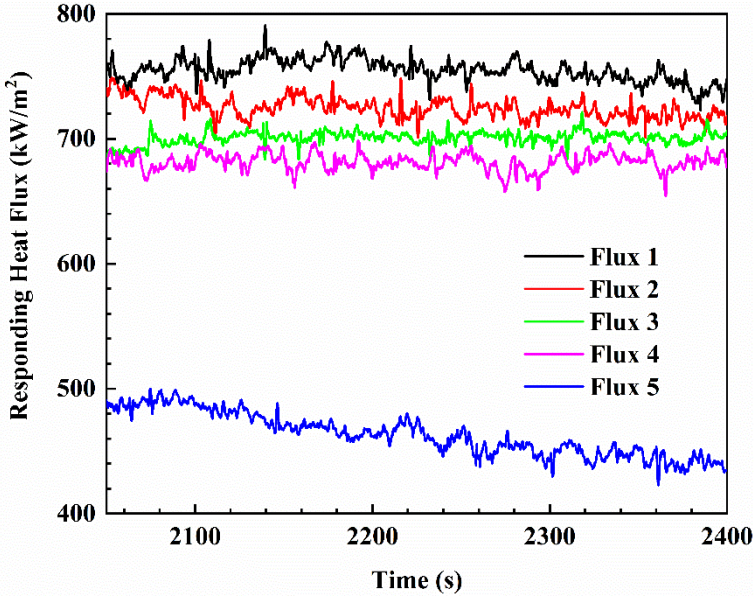

Fig. 9 Heat fluxes of five mould fluxes determined in IET experiment

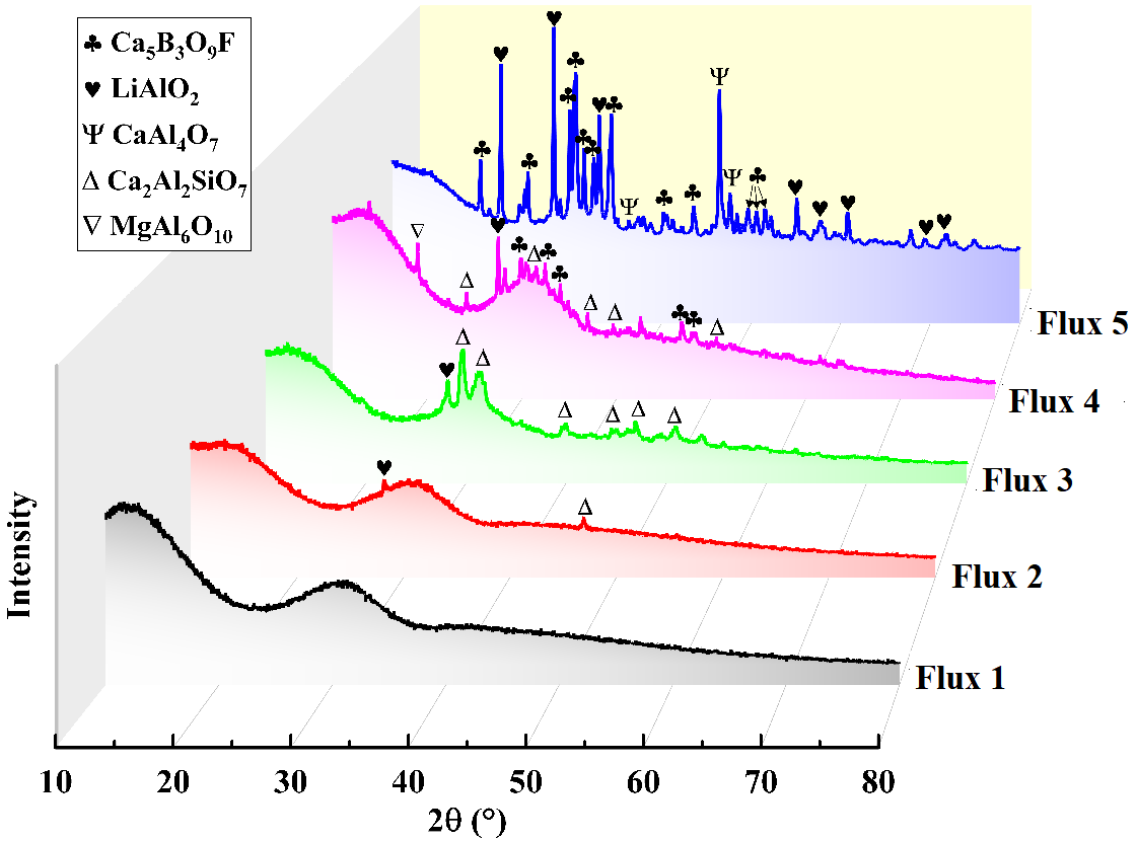

Fig. 10 XRD patterns of the flux discs after IET experiments

Flux discs after IET experiments were subjected to XRD analysis; the results are shown in **Figure 10**. Flux 1 was fully amorphous, and Flux 2 was basically amorphous with a couple of very small peaks. With the increase of Al_2O_3/SiO_2 ratio, more crystal peaks appeared with the increased intensity, indicating the crystallization tendency of the mould flux was enhanced. The main phases identified were $Ca_2Al_2SiO_7$ for Flux 3; $LiAlO_2$, $MgAl_6O_{10}$, $Ca_2Al_2SiO_7$ and $Ca_5B_3O_9F$ for Flux 4; and $LiAlO_2$, $Ca_5B_3O_9F$, $CaAl_4O_7$ for Flux 5.

DISCUSSION

Experimental results showed that the change of Al_2O_3/SiO_2 ratio led to the variation of flux properties. With the increase of Al_2O_3/SiO_2 ratio, the flux melting temperature and viscosity increased, while the heat transfer decreased. The dominate silicate structure shifted to the aluminate structure, affecting the viscosity. The increasing Al_2O_3/SiO_2 ratio raised the crystallisation tendency of fluxes, which explains a decreasing trend of heat transfer and an increasing flux melting temperatures.

Effect of Al_2O_3/SiO_2 ratio on the structure and the viscosity of mould fluxes

According to the results of Raman spectroscopy shown in **Figures 5** to **6**, the increase of Al_2O_3/SiO_2 ratio, i.e., the increase of Al_2O_3 content and the decrease of SiO_2 content, promoted the formation of aluminate structural units, e.g., AlF_6, AlO_6, and Al-O-Al, but decreased the Al-O-Si linkage. Both Al-O-Al and Al-O-Si were 3-D structure components, while AlF_6, and AlO_6 were 2-D structure components in the melt with octahedral coordination. The increased Al-O-Al 3-D structural units lead to an increased degree of polymerisation, while the decreased Al-O-Si (3-D structure) and the enhanced AlF_6 and AlO_6 2-D structural units result in a decreased degree of polymerisation. Overall, the increasing Al_2O_3 content in the flux facilitated the accumulation of Al-related network.

In addition to Al-O related structures, with the increase of Al_2O_3/SiO_2 ratio, the silicate structures were also changed (**Figures 5** and **6**). The area fraction of Q^2 increased, and the area fraction of Q^0 decreased. There was even Q^3 presented in Flux 5. The degree of polymerisation referring to the silicate structure can be characterised by non-bridging oxygen per silicon NBO/Si, which is determined as:

$$\mathrm{NBO/Si} = 4X_{Q^0} + 3X_{Q^1} + 2X_{Q^2} + X_{Q^3} \quad (3)$$

The values of NBO/Si are shown in **Figure 11** where NBO/Si decreased slightly with the increase in the Al_2O_3/SiO_2 ratio from 0.7 to 10.8, indicating an increased polymerisation of silicate structures. [Zhang et. al. 2008] also found that the increase in Al_2O_3/SiO_2 ratio increased the $[SiO_4]$-tetrahedral structure and therefore increased polymerisation.

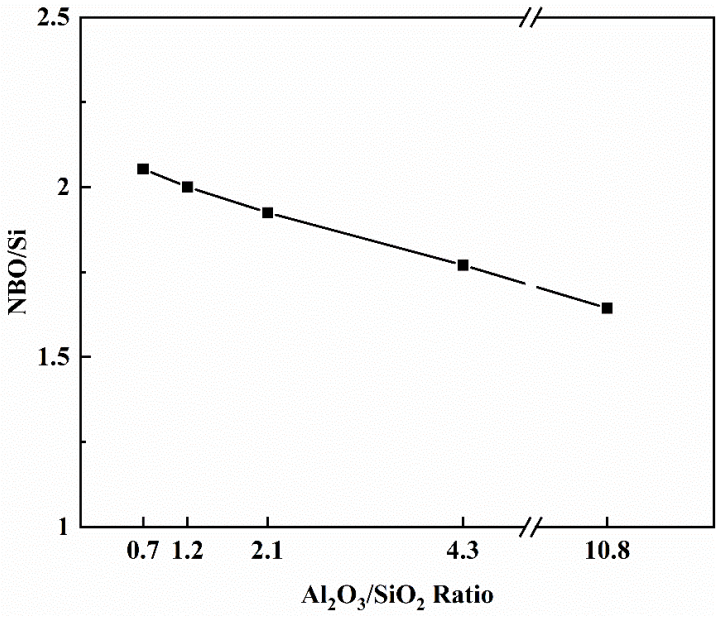

Fig. 1 Values of NBO/Si as a function of Al_2O_3/SiO_2 ratio

For borate region, within the range of Al_2O_3/SiO_2 ratio from 0.7 to 2.1, changes of the area fractions of borate-related structural units were marginal compared to those of aluminate-related and silicate-related structural units. With further increasing Al_2O_3/SiO_2 ratio from 2.1 to 10.8, the area fraction of borate-related structures increased, correlating with the decrease of SiO_2 content. Silicate and aluminate structure can be treated as the backbone of the whole melt [Mills 1993]. The borate structure change is much less significant than those of aluminate and silicate structures. The effect of Al_2O_3/SiO_2 ratio on polymerisation of the whole flux depends mainly on the combined contribution of aluminate and silicate structures.

The viscosity of mould fluxes is generally correlated well with the flux structures, or more specifically, with the degree of polymerisation. As shown in **Figure 3**, viscosity sharply increased first when Al_2O_3/SiO_2 ratio increased from 0.7 to 1.2, but then rapidly decreased when Al_2O_3/SiO_2 ratio further increased from 1.2 to 10.8. This observation indicates that the flux polymerisation experiences a turning point when Al_2O_3/SiO_2 reaches 1.2 (Al_2O_3 20.5 mass pct, Flux 2). Similar results were also reported by Kim et al. [Kim et al. 2012] in their work on $CaO\text{-}SiO_2\text{-}Al_2O_3\text{-}Na_2O\text{-}Li_2O$ flux and Chen et al. [Chen et al. 2019] on $CaO\text{-}SiO_2\text{-}MgO\text{-}Al_2O_3$ slag where they found that the viscosity initially increased to a maximum at about 20 mass pct Al_2O_3 and then decreased with further addition of Al_2O_3. This phenomenon cannot be explained by the decreased NBO/Si shown in Figure 11 which indicates an increased degree of polymerisation. Similarly, NBO/T ratio (non-bridging O/tetragonal O) calculated using the following equation:

$$\frac{NBO}{T} = \frac{2\left(X_{CaO}+X_{MgO}+X_{Na2O}+X_{Li2O}-X_{Al2O3}-X_{B2O3}\right)}{X_{SiO2}+2X_{Al2O3}+2X_{B2O3}} \quad (4)$$

also showed the decreased NBO/T with the Al_2O_3/SiO_2 ratio (Figure 12). Therefore, there are other factors to cause this change.

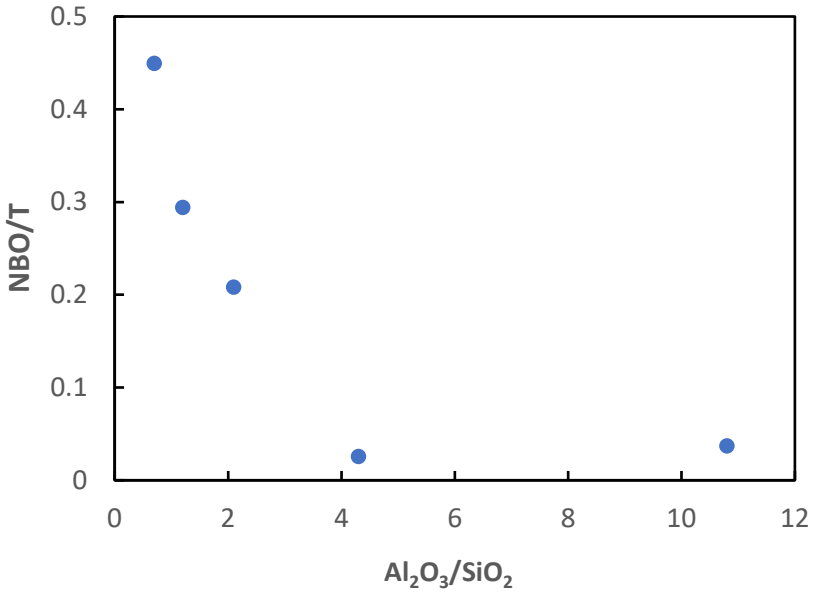

Figure 12. NBO/T vs Al_2O_3/SiO_2

When Al_2O_3 is introduced into the silicate network, the Al^{3+} ions can be absorbed into the silicate structure, exhibiting fourfold coordination like Si^{4+}. However, there is a charge difference between Al^{3+} and Si^{4+} which needs to be compensated by M^{2+} and/or M^{+} ions, e.g. Na^{+}, Li^{+}, Ca^{2+} and Mg^{2+}. Thus, Al_2O_3 additions act principally as network formers, e.g. in the case of fluxes 1 and 2. However, when large amounts of Al_2O_3 are added to the slag (e.g. fluxes 4 and 5), the Al^{3+} ions can also act as network breakers forming five- or sixfold coordination [Stebbins et al. 1992]. Therefore this phenomenon can be attributed to the amphoteric effect of Al_2O_3, serving as a network former when Al_2O_3 content is low but a network modifier when its concentration is high. The turning point is when the Al/M ratio ($=2X_{Al2O3}/(2X_{Na2O}+2X_{Li2O}+X_{CaO}+X_{MgO})$) approaches 1 which is the case of flux 4 (Al/M = 0.9).

Chen et al. [Chen et al. 2019] found a transition point (minimum) in the molar Gibbs energy of the mixing of the $CaO\text{-}SiO_2\text{-}MgO\text{-}Al_2O_3$ slag system at 17 mass pct Al_2O_3. This calculated transition point is close to the viscosity turning point observed in this work and other reports [Zhang et al. 2008, Kim et al. 2012].

Effect of Al_2O_3/SiO_2 ratio on heat transfer of mould flux

XRD analysis of isothermally treated fluxes in **Figures 7** and **8** reveals that changing Al_2O_3/SiO_2 ratio changes the phase composition of the fluxes. For the highest SiO_2 content (Flux 1, lowest Al_2O_3/SiO_2 ratio), caspidine appeared which is a key component of $CaO\text{-}SiO_2\text{-}Al_2O_3$-based commercial mould fluxes. Because of high SiO_2 concentration, this flux and Flux 2 were converted to predominantly amorphous phases after a fast cooling after the heat transfer measurements (**Figure 10**). In the flux 3 with Al_2O_3/SiO_2 ratio 2.1, no cuspidine was observed but only $Ca_2Al_2SiO_7$ was detected at both 900 and 1000°C and in the samples after heat transfer measurements (**Figure 10**). Further increasing Al_2O_3/SiO_2 ratio to 4.3 and 10.8 led to a more complex multi-crystal phase formation, including $LiAlO_2$, $MgAl_6O_{10}$, $CaSiO_3$ or $Ca_5B_3O_9F$ (**Figures 7, 8** and **10**). Clearly, increasing Al_2O_3/SiO_2 ratio increases significantly the crystallisation tendency of the fluxes.

Heat transfer of mould flux depends strongly on flux crystallinity and types of crystals. With the increase in Al_2O_3/SiO_2 ratio, the heat flux through the slag film decreased gradually first (Flux 1 to Flux 4) and then dropped tremendously (Figure 9, Flux 5). As discussed above, increasing Al_2O_3/SiO_2 ratio increased flux crystallinity which therefore led to the decrease in heat transfer because of the heat scattering effect by grain boundaries and defects. The higher the crystallinity, the lower the heat flux. The significant decrease in the heat flux when Al_2O_3/SiO_2 is 10.8 could be also related to the crystals morphology although it is not the crucial factor in the heat transfer.

Flux selection in terms of Al_2O_3/SiO_2 ratio

As discussed above, $CaO\text{-}SiO_2$-based mould fluxes cannot be used for casting of high-Al steel because of the strong flux-steel reaction, leading to the significant variation of the flux properties demonstrated in this work. Above discussion reveals that the turning point of the viscosity reflects the difference in the flux properties and structure between $CaO\text{-}SiO_2$ based fluxes and $CaO\text{-}Al_2O_3$ based mould fluxes. This work also indicates that when SiO_2 is very low, e.g., Flux 5, flux crystallisation is too strong to provide an appropriate lubrication. Therefore, Flux 3 (Al_2O_3/SiO_2 = 2.1 mass pct ratio) and Flux 4 (Al_2O_3/SiO_2 = 4.3 mass pct ratio) could be considered to provide suitable structure and crystallinity to achieve optimal flux properties. By minimising the flux-steel reaction, the lower SiO_2 flux is preferred, i.e., Flux 4.

CONCLUSIONS

The effect of Al_2O_3/SiO_2 ratio on structure, viscosity, crystallization behaviour and heat transfer of $CaO\text{-}Al_2O_3\text{-}SiO_2\text{-}B_2O_3\text{-}Na_2O\text{-}Li_2O\text{-}MgO\text{-}F$ fluxes was investigated. The major findings are summarized as follows:

- Flux melting temperatures increase with the increase in the Al_2O_3/SiO_2 ratio.
- Viscosity of the flux melts increase significantly with the increasing Al_2O_3/SiO_2 ratio from 0.7 to 1.2, reaching the maximum value, and then decrease with the further increase of Al_2O_3/SiO_2 ratio. Raman spectroscopy analysis revealed that the change of Al_2O_3/SiO_2 ratio leads to the change of flux structures. The turning point for viscosity can be attributed to the amphoteric effect of Al_2O_3, serving as a network former when Al_2O_3 content is low but a network modifier when its concentration is high.
- XRD analysis showed that increasing Al_2O_3/SiO_2 ratio increased crystallisation tendency of the fluxes. Heat transfer measurement by IET revealed that increasing Al_2O_3/SiO_2 ratio led to the decrease in the heat flux which is correlated well with the increased crystallinity of the flux.
- It can be concluded from this work that Al_2O_3/SiO_2 = 4.3 (SiO_2 7 mass pct, Flux 4) is the best candidate among studied $CaO\text{-}Al_2O_3$-based mould fluxes to provide optimal flux properties but minimise the flux-steel reaction.

ACKNOWLEDGEMENTS

Financial supports from Baosteel-Australia Joint Research and Development Centre (BAJC) and Australian Research Council (ARC) Industrial Transformation Hub are greatly acknowledged.

REFERENCES

Brandaleze, E., Di Gresia, G., Santini, L., Martín, A. and Benavidez, E., **2012,** Mould fluxes in the steel continuous casting process, in *Science and Technology of Casting Processes*, 1st ed., InTech, pp. 205-233

Chen, Z.; Wang, H.; Sun, Y.; Liu, L.; Wang, X., **2019.** Insight into the Relationship Between Viscosity and Structure of $CaO\text{-}SiO_2\text{-}MgO\text{-}Al_2O_3$ Molten Slags. *Metallurgical and Materials Transactions B 50* (6), 2930-2941

Cho, J.W, Blazek K., Frazee M., Yin H., Park J.H., and Moon S.W. **2013.** *ISIJ Int*., *53,* 62.

Chung Y, and Cramb A.W. **2000.** *Metall. Mater. Trans. B*, *31B,* 957.

Gao, E.; Wang, W.; Zhang, L., **2017.** Effect of alkaline earth metal oxides on the viscosity and structure of the $CaO\text{-}Al_2O_3$ based mold flux for casting high-al steels. *Journal of Non-Crystalline Solids 473*, 79-86

Gao, J.; Wen, G.; Huang, T.; Bai, B.; Tang, P.; Liu, Q., **2016.** Effect of slag-steel reaction on the structure and viscosity of $CaO\text{-}SiO_2$-based mold flux during high-Al steel casting. *Journal of Non-Crystalline Solids 452*, 119-124

Gao, J.; Wen, G.; Huang, T.; Bai, B.; Tang, P.; Liu, Q., **2016.** Effect of Al Speciation on the Structure of High-Al Steels Mold Fluxes Containing Fluoride. *Journal of the American Ceramic Society 99* (12), 3941-3947

Kamitsos, E. I.; Karakassides, M. A.; Chryssikos, G. D., **1987.** Vibrational spectra of magnesium-sodium-borate glasses. 2. Raman and mid-infrared investigation of the network structure. *The Journal of Physical Chemistry 91* (5), 1073-1079

Kang, Y.B, Kim M.S., Lee S.W., Cho J.W., Park M.S., and Lee H.G. **2013.** *Metall. Mater. Trans. B*, *44B,* 309.

Kim, H.; Matsuura, H.; Tsukihashi, F.; Wang, W.; Min, D. J.; Sohn, I., **2012.** Effect of Al_2O_3 and CaO/SiO_2 on the Viscosity of Calcium-Silicate–Based Slags Containing 10 Mass Pct MgO. *Metallurgical and Materials Transactions B 44* (1), 5-12

Kim, G. H.; Sohn, I., **2012.** Effect of Al_2O_3 on the viscosity and structure of calcium silicate-based melts containing Na_2O and CaF_2. *Journal of Non-Crystalline Solids 358* (12-13), 1530-1537

Kim, M S, Lee, S W, Cho J W., Park M.S., Lee H.G., and Kang Y.B. **2013.** *Metall. Mater. Trans. B*, *44B,* 299.

Kim, G. H.; Sohn, I., **2014.** Role of B_2O_3 on the Viscosity and Structure in the CaO-Al_2O_3-Na_2O-Based System. *Metallurgical and Materials Transactions B 45* (1), 86-95

Kim, T. S.; Park, J. H., **2014.** Structure-Viscosity Relationship of Low-silica Calcium Aluminosilicate Melts. *ISIJ International 54* (9), 2031-2038

Ma, N.; You, J.; Lu, L.; Wang, J.; Wang, M.; Wan, S., **2018.** Micro-structure studies of the molten binary K_3AlF_6–Al_2O_3 system by in situ high temperature Raman spectroscopy and theoretical simulation. *Inorganic Chemistry Frontiers 5* (8), 1861-1868

McMillan, P.; Piriou, B., **1983.** Raman spectroscopy of calcium aluminate glasses and crystals. *Journal of Non-Crystalline Solids 55* (2), 221-242

Mills, K. C., **1993.** The Influence of Structure on the Physico-chemical Properties of Slags. *ISIJ International 33* (1), 148-155

Park, J. H.; Min, D. J.; Song, H. S., **2002.** Structural Investigation of CaO-Al_2O_3 and CaO-Al_2O_3-CaF_2 Slags *via* Fourier Transform Infrared Spectra. *ISIJ International 42* (1), 38-43

Park J.Y., Kim G.H., Kim J.B., Park S. and Sohn I. **2016.** *Metallurgical and Materials Transactions B*, *47,* 2582.

Stebbins, J. F.; Farnan, I; Xue, X. **1992**. Chem. Geol. 96, 371-385.

Wang W and Cramb A. **2005.** *ISIJ International*, *45,* 1864.

Yang, J, Zhang J., Sasaki Y., Ostrovski O., Zhang C., Cai D. and Kashiwaya Y. **2017.** *Metall. Mater. Trans. B, 48B,* 2077.

Yang, J, Zhang J., Ostrovski O., Zhang C. and Cai D. **2018.** *Metallurgical and Materials Transactions B*, *50,* 291.

Zhang, Z.; Wen, G.; Tang, P.; Sridhar, S., **2008.** The Influence of Al_2O_3/SiO_2 Ratio on the Viscosity of Mold Fluxes. *ISIJ International 48* (6), 739-746

Zheng, K.; Zhang, Z.; Liu, L.; Wang, X., **2014.** Investigation of the Viscosity and Structural Properties of CaO-SiO_2-TiO_2 Slags. *Metallurgical and Materials Transactions B 45* (4), 1389-1397

Zhou, L, Wang W., and Zhou K. **2015.** *Metallurgical and Materials Transactions E*, *2,* 99.

Zhou, L, Li J., Wang W., and Sohn I. **2017.** *Metall. Mater. Trans. B*, *48B,* 1943.